The FASEB Journal

FASEB
Federation of American Societies for Experimental Biology

RESEARCH ARTICLE OPEN ACCESS

NERP-4–Deleted VGF Impairs β-Cell Granulogenesis and Insulin Secretion

Weidong Zhang[1,2] | Yuki Nakazato[3] | Naoto Minamino[4] | Nobuaki Okumura[2] | Ayako Miura[5] | Takefusa Tarusawa[6] | Hiroki Mizukami[6] | Hideyuki Sakoda[2] | Masamitsu Nakazato[7]

[1]Department of Veterinary Anatomy, Faculty of Agriculture, University of Miyazaki, Miyazaki, Miyazaki, Japan | [2]Laboratory of Biomolecular Analysis, Institute for Protein Research, The University of Osaka, Osaka, Japan | [3]Division of Respirology, Rheumatology, Infectious Diseases, and Neurology, Department of Internal Medicine, Faculty of Medicine, University of Miyazaki, Miyazaki, Miyazaki, Japan | [4]Department of Molecular Pharmacology, National Cerebral and Cardiovascular Center Research Institute, Osaka, Japan | [5]Department of Bioregulatory Sciences, Faculty of Medicine, University of Miyazaki, Miyazaki, Miyazaki, Japan | [6]Department of Pathology and Molecular Medicine, Biomedical Research Center, Hirosaki University Graduate School of Medicine, Hirosaki, Japan | [7]Forefront Research Center, Graduate School of Science, The University of Osaka, Osaka, Japan

Correspondence: Weidong Zhang (weidong_zhang@med.miyazaki-u.ac.jp) | Masamitsu Nakazato (nakazato@med.miyazaki-u.ac.jp)

Received: 16 July 2025 | **Revised:** 8 October 2025 | **Accepted:** 8 December 2025

Keywords: granulogenesis | insulin | NERP-4 | VGF | β cell

ABSTRACT

Neuroendocrine regulatory peptide-4 (NERP-4) processed from the granin protein VGF functions as a positive allosteric modulator that acts on the amino acid transporter SNAT2 expressed on pancreatic β cells. NERP-4 promotes insulin secretion and β-cell maintenance. We studied the effects of NERP-4–deleted VGF ($VGF^{\triangle NERP\text{-}4}$) on β-cell functions in MIN6-K8 β cells and CRISPR-Cas9–designed mouse islets. $VGF^{\triangle NERP\text{-}4}$ exhibited reduced insulin secretion and disrupted β-cell maintenance. Notably, $VGF^{\triangle NERP\text{-}4}$ caused defective insulin granule formation via insulin accumulation in the *trans*-Golgi network, thereby reducing replenishment of insulin granule stores in the second-phase insulin secretion. These findings are comparable to those obtained in *Vgf* knockdown. NERP-4 administration to $VGF^{\triangle NERP\text{-}4}$ β cells restored β-cell maintenance but not insulin granule formation. NERP-4 was reduced in the islets of patients with type 2 diabetes mellitus. NERP-4 plays a role in β-cell viability and the NERP-4 region is critical for VGF structure in the context of granulogenesis, thereby providing new insights into the role of NERP-4 in β-cell biology.

1 | Introduction

Insulin is stored in granules of β cells and secreted in response to multiple stimuli, including nutrients, hormones, local signaling, and neuronal inputs. Proinsulin synthesized in the rough endoplasmic reticulum (ER) is transported to the Golgi complex and sorted at the *trans*-Golgi network [1, 2]. It is then packed into immature secretory granules, together with granin protein family members VGF, chromogranin A, and chromogranin B [3–5]. VGF, an acidic protein also named secretogranin VII, comprises 615 (human) or 617 (mouse/rat) amino acids and aggregates in the secretory granules under low pH conditions [6–9]. These aggregates facilitate proinsulin condensation and insulin maturation in the secretory granules [5]. Mature secretory granules are mobilized to fuse with the plasma membrane and deliver insulin to the bloodstream.

Abbreviations: ATP, Adenosine triphosphate; Cas9, CRISPR-associated protein 9; CRISPR, clustered regularly interspaced short palindromic repeats; DCFH2-DA, 2,7-dichlorodihydrofluorescein diacetate; DMEM, Dulbecco's modified eagle's medium; Dz, diazoxide; ER, endoplasmic reticulum; GSIS, glucose-stimulated insulin secretion; ND, non-diabetes individuals; NERP-4, neuroendocrine regulatory peptide-4; PCs, Prohormone convertases; SNAT2, sodium-coupled neutral amino acid transporter 2; T2DM, type 2 diabetes mellitus; VGF, VGF nerve growth factor inducible.

Weidong Zhang and Yuki Nakazato contributed equally to this work.

Granin proteins act on trafficking secretory granules and regulate granule mobility, secretion potential, and degradation [10]. They also function as multiple peptide precursors. Prohormone convertases (PCs) and carboxypeptidases are also packed into secretory granules where these enzymes process precursor proteins to biologically active peptides. VGF is processed by PC1/3 and PC2 into a variety of peptides, including insulinotropic peptides NERP-2, TLQP-21, TLQP-62, and AQEE-30 [11–14]. Our recent study has demonstrated that NERP-4, another VGF-derived insulinotropic peptide corresponding to VGF489–507 in mice, acts as a positive allosteric modulator on the amino acid transporter SNAT2/SLC38A2 expressed on β cells [15]. NERP-4 enhanced the uptake of neutral amino acids glutamine, alanine, and proline, thereby contributing to β-cell function and maintenance [15]. NERP-4 neutralization with an anti–NERP-4 IgG reduced insulin secretion and β-cell viability [15].

VGF loss-of-function studies in isolated mouse islets and conditional knockout mice presented defective secretory granule biogenesis and proinsulin processing [9]. Here, we investigated the biological significance of NERP-4–deleted VGF ($VGF^{\triangle NERP\text{-}4}$) in β-cell function and viability. We generated two distinct models of $VGF^{\triangle NERP\text{-}4}$: one of mouse insulinoma–derived MIN6-K8 cells and the other of islets isolated from CRISPR/Cas9–designed mice. Additionally, we studied the structural importance of the NERP-4 region in VGF–mediated granulogenesis in β cells. To explore whether NERP-4 reduction is related to diabetes pathogenesis, we investigated the NERP-4 immunoreactivity in the islets of patients with type 2 diabetes mellitus. We demonstrate that NERP-4 plays a role in β-cell viability and that the NERP-4 region is critical for the function of VGF as a granin protein.

2 | Materials and Methods

2.1 | Cultured Cells

MIN6-K8 cells were provided by Dr. Jun-ichi Miyazaki (The University of Osaka). They are mouse insulinoma–derived β cells [16] that have been used to study the mechanism of secretory granule formation and insulin secretion [15, 17–19]. They were maintained in Dulbecco's modified Eagle's medium (DMEM; 044–29 765; Wako) supplemented with 10% fetal bovine serum (FBS), 25 mM glucose, 4 mM glutamine, 100 U/mL benzylpenicillin, and 100 mg/mL streptomycin at 37°C in a humidified atmosphere of 5% CO_2.

2.2 | Patients and Specimens

Human pancreatic tissues were studied according to the guidelines of the Ethics Committee on Human Research Samples at the Japanese Society of Pathology after approval by the ethics committee of Hirosaki University School of Medicine (approval number #2013–235, 2024–092). The study conforms to the provision of the Declaration of Helsinki. All participants studied gave their informed consents prior to their inclusion in the study. A total of 34 patients who underwent autopsy at Hirosaki University Hospital from 2012 to 2016 were analyzed retrospectively. Major clinical characteristics were obtained from the clinical records. The specimens from 14 non-diabetes individuals and 20 patients with type 2 diabetes mellitus were used for immunofluorescent histological analyses.

2.3 | si*RNA Treatment*

MIN6-K8 cells (2×10^5 cells/well in 48-well plates) were treated for 72 h with mouse *Vgf* siRNA (20 pmol/mL; s117809; Thermo Fisher Scientific) or siSCR (4 390 843; Thermo Fisher Scientific) using Lipofectamine RNAiMAX Reagent (Thermo Fisher Scientific). Knockdown and knockin efficacy was studied by western blot and PCR analyses.

2.4 | *Transfection of Vgf*-Knocked Down *MIN6-K8 Cells With* Vgf^{full} *or* $Vgf^{\triangle Nerp\text{-}4}$

Hypothalamic cDNA from CRISPR-Cas9–designed $Nerp\text{-}4^{-/-}$ mice and their littermates were used to generate vectors. Full-length (Vgf^{full}) and *Nerp-4*–deleted ($Vgf^{\triangle Nerp\text{-}4}$) mouse *Vgf* were amplified by PCR and inserted into the *Hind* III and *Eco*RI sites of a pcDNA3.1 (+) vector (Thermo Fisher Scientific). MIN6-K8 cells were transfected with pcDNA3.1 (+) vector containing mock, Vgf^{full}, or $Vgf^{\triangle Nerp\text{-}4}$ using ViaFect (Promega) for 36 h (Figure 1a). In the palmitate experiments (Figure 4c), the cells were treated with 0.5 mM palmitate in DMEM for 24 h after Vgf^{full} or $Vgf^{\triangle Nerp\text{-}4}$ transfection. NERP-4 at a final concentration of 10^{-10} M was administered to the $Vgf^{\triangle Nerp\text{-}4}$ + NERP-4 administration group 12, 24, and 36 h after. $Vgf^{\triangle Nerp\text{-}4}$ transfection.

2.5 | Cell Viability Assay

MIN6-K8 cells were treated as shown in Figure 1a prior to use. Five groups of the cells were maintained in DMEM supplemented with 10% FBS, 25 mM glucose, 4 mM glutamine, 100 U/mL benzylpenicillin, and 100 mg/mL streptomycin at 37°C in a humidified atmosphere of 5% CO_2. Cell viability was evaluated using a Cell Counting Kit-8 (Dojindo).

2.6 | ATP Assay

The five groups of MIN6-K8 cells in Figure 1a were preincubated with 2.8 mM glucose for 30 min and then incubated with 16.7 mM glucose for 30 min. They were then lysed and the ATP content was measured using a Colorimetric/Fluorometric Assay Kit (BioVision).

2.7 | Measurement of Oxidants

MIN6-K8 cells were seeded on a 96-well black plate (Corning), and the five groups of the cells in Figure 4c were administered 500 500 μM sodium palmitate (Sigma-Aldrich) for 24 h. They were then incubated with 50 μM 2,7-dichlorodihydrofluorescein diacetate (DCFH2-DA, Dojindo) for 30 min at 37°C to detect the oxidants produced in the cells [20]. Fluorescence intensity was measured using a VICTOR Nivo (PerkinElmer) with excitation and emission at 488 nm and 522 nm, respectively.

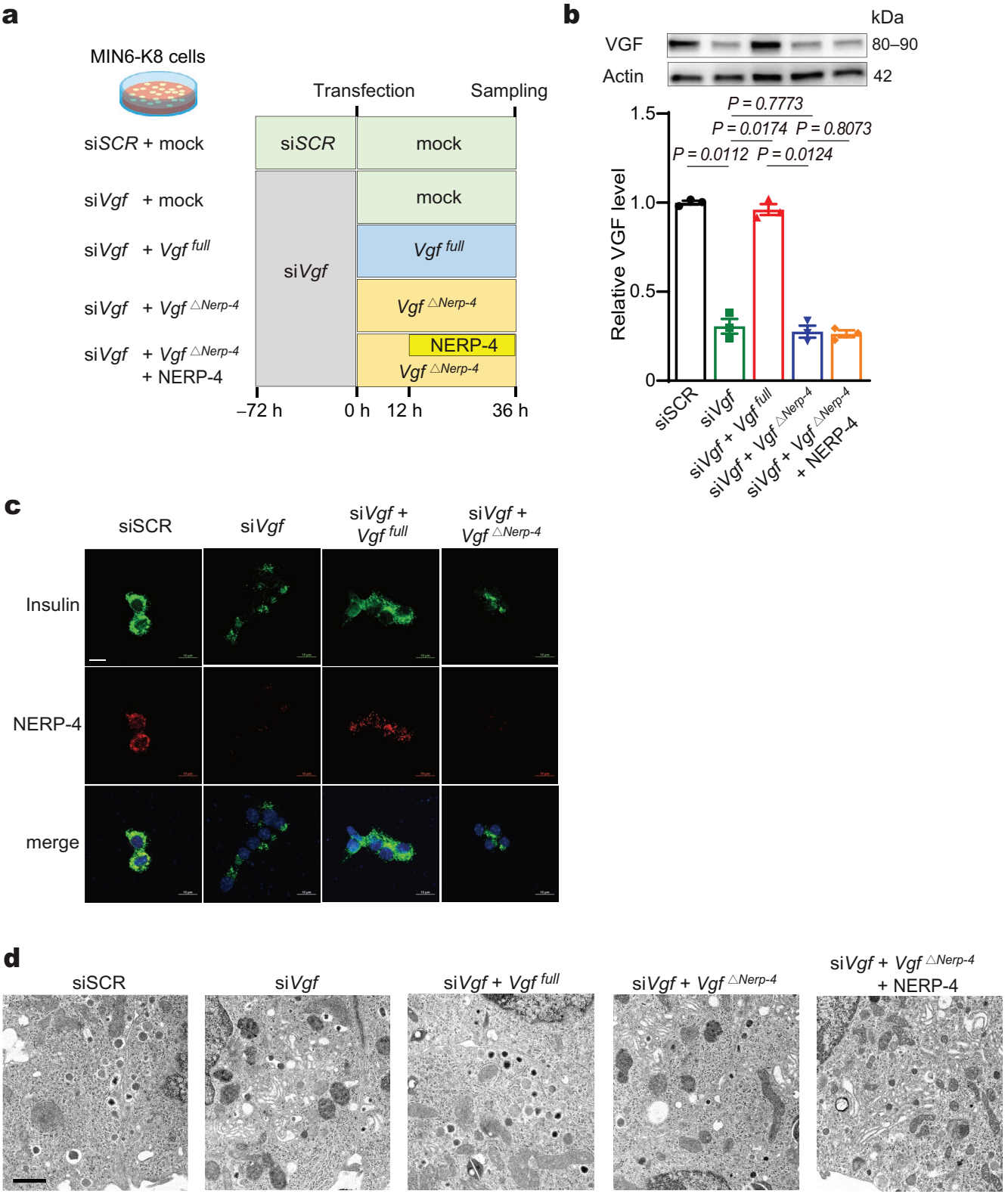

FIGURE1 | NERP-4 deletion reduces insulin storage. (a) si*Vgf*–MIN6-K8 cells were transfected with Vgf^{full} or $Vgf^{\triangle NERP\text{-}4}$ for 36 h before use. NERP-4 was administered twice at 12 and 24 h after $Vgf^{\triangle NERP\text{-}4}$ transfection. (b) Western blot analysis of VGF after transfection ($n = 3$). (c) Representative immunostaining of insulin and NERP-4 in MIN6-K8 cells ($n = 8$ areas per group). (d) Representative transmission electron micrograph of MIN6-K8 cells ($n = 12$ sections per group). (e, f) Box plots showing the numbers ($n = 15$) and diameters ($n = 317$, 137, 191, 116, and 148) of insulin storage granules. (g) Insulin content ($n = 4$). (h) GSIS ($n = 4$). (i) Proinsulin/insulin ratio ($n = 4$). Representative results of two independent experiments (b–i). Data are presented as the mean ± s.e.m. (b, e–i). One-way ANOVA and Tukey's multiple comparisons test (b, e–i). Scale bars, 10 μm (c), 1 μm (d).

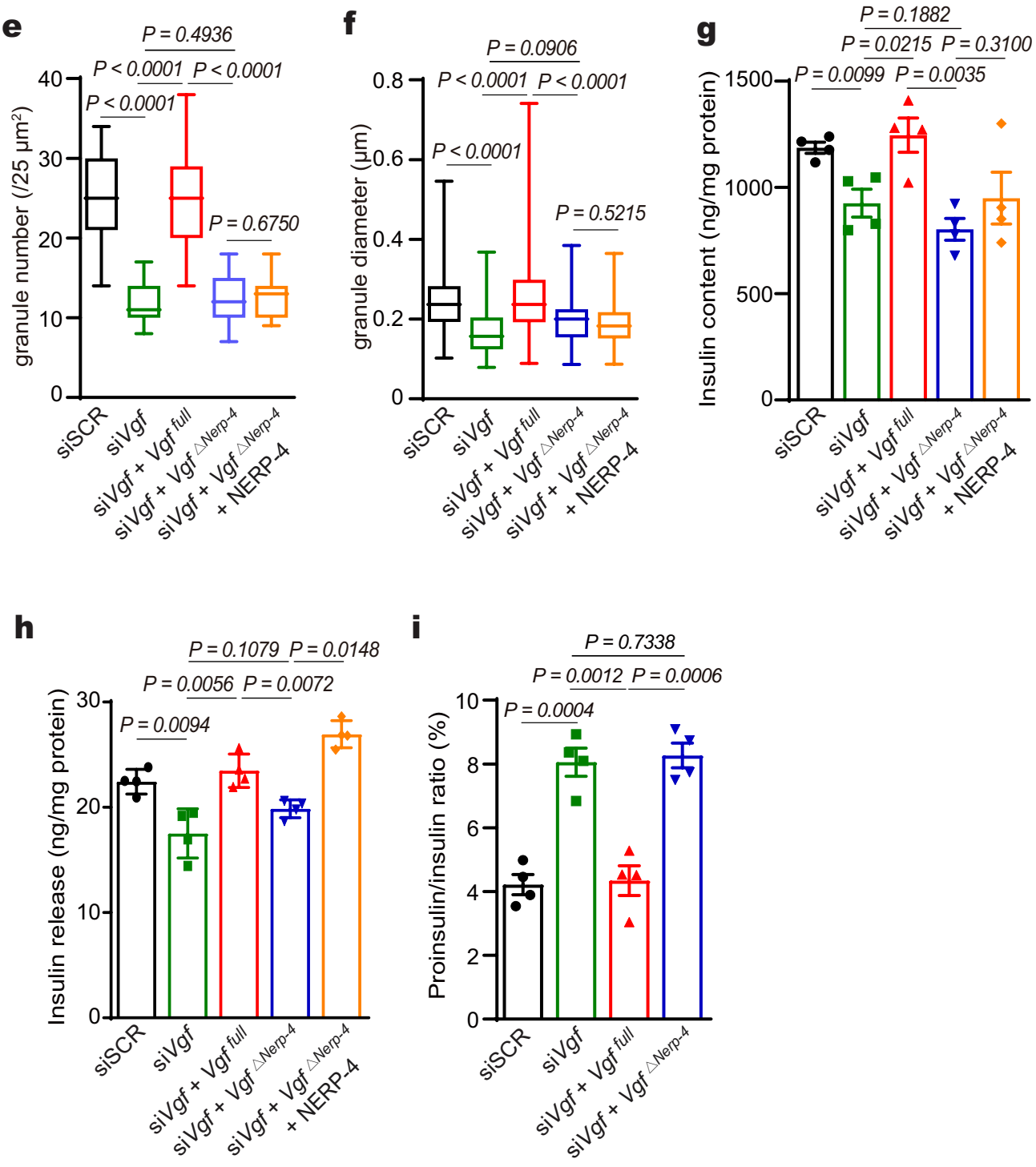

FIGURE 1 | (Continued)

2.8 | Generation of Systemic Nerp-4$^{-/-}$ Mice

Nerp-4$^{-/-}$ mice were generated using CRISPR-Cas9 technology (Trans Genic Inc.). The sequences of the gRNAs used were as follows: gRNA84N; 5′-GAGGCGGCACCGGCTCG GGA-3′, gRNA84C; 5′-CGGAGAGCGGACATGGGTCG-3′. These sequences were inserted into a plasmid containing the CAG-promoter–driven *hCas9* coding sequence. To introduce a deletion mutation, single-stranded oligo DNA with a 100 bp homologous arm identical to the upstream and downstream sequences of the region to be deleted was designed and synthesized (Ultramer oligos; Integrated DNA Technologies) as donor DNA. The expression vector (2 pL of 5 ng/μL) and donor DNA (100 ng/μL) were microinjected into fertilized C57BL/6N eggs. Deletion mutant alleles were detected by direct sequencing. To confirm gene deletion at the mRNA level, PCR was carried out using KOD FX (Toyobo) with the following primers: F11904, 5′-CCCCGCTAGCTGTTCGCCGAGGAGGAGGAC-3′; and R12430, 5′-CCCCGAATTCCTCCAGATCCGGATGGTGGC-3′. The sizes of the PCR products from WT and NERP-4 KO mice

were 547 bp and 490 bp, respectively. The mice were maintained under controlled temperature (21°C–23°C) and light (light on: 08:00–20:00) conditions and were given free access to a standard diet (CE-2; CLEA Japan) and water. Male mice were used for the experiments. All animal experiments were performed in accordance with the Japanese Physiological Society guidelines for animal care and were approved by the Ethics Committee on Animal Experimentation of the University of Miyazaki. The mice under *ad libitum* conditions were humanely euthanized via intraperitoneal injection with a combination anesthetic consisting of 0.3 mg/kg medetomidine, 4.0 mg/kg midazolam, and 5.0 mg/kg butorphanol. Blood, pancreas, and islets were collected after euthanasia.

2.9 | Quantitative Real-Time PCR (RT-PCR)

mRNA was extracted from MIN6-K8 cells and mouse islets using a Ribopure Kit (Thermo Fisher Scientific). First-strand cDNA was synthesized using high-capacity cDNA reverse transcription kits (Applied Biosystems). Quantitative RT-PCR was performed on a Thermal Cycler Dice Real Time System II (Takara Bio) using TaqMan Fast Universal PCR Master Mix (Thermo Fisher Scientific) and TaqMan/Applied Biosciences primers shown in Table S1. Expression levels in the PCR products were normalized to that of glyceraldehyde3-phosphate dehydrogenase (*Gapdh*) mRNA.

2.10 | Antibody Preparation

Anti–NERP-4 antibody was prepared by immunizing rabbits against mouse acetyl NERP-4[8–19 amino acids], as described previously [15]. Anti-VGF antibody was prepared by immunizing rabbits against mouse cysteinyl VGF[610–617 amino acids] [21] coupled with maleimide-activated keyhole limpet hemocyanin (Pierce). The VGF IgG was purified over a Protein G Sepharose 4 Fast Flow column (Merck Millipore).

2.11 | Immunohistochemistry

The anesthetized mice were transcardially perfused with 100 mL of ice-cold heparinized phosphate-buffered saline (0.1 M, pH 7.4) and then with 50 mL of ice-cold 4% paraformaldehyde. Mouse pancreata were infiltrated with 4% paraformaldehyde overnight at 4°C and embedded in optimal cutting temperature compound (Sakura Finetek). MIN6-K8 cells were fixed with 4% paraformaldehyde for 15 min at room temperature (RT). Immunohistochemistry of human pancreata was performed with 4 μm-thick sections of paraffin-embedded tissue specimens. After dewaxing steps, the antigen retrieval was performed with a citrate-based antigen retrieval solution (pH 6.0; H-3300, Vector Laboratories). For double immunofluorescence staining [15], sections of human and mouse pancreata or MIN6-K8 cells were incubated overnight at 4°C with the primary antibodies. They were then incubated for 1 h at RT with corresponding Alexa Fluor 488– and 594–conjugated secondary antibodies. The samples were observed under an AX-7 fluorescence (Olympus) or C2 confocal (Nikon) microscope. Fluorescence intensity and area were measured using ImageJ software (National Institutes of Health). The antibodies and staining conditions used are described in Table S1.

2.12 | Western Blotting

Proteins extracted from MIN6-K8 cells and mouse islets were analyzed by western blotting with the indicated antibodies (Table S1), as described previously [22]. The cells and islets were ruptured with NP40 lysis buffer (MedChemExpress). The protein samples were resolved by SDS–PAGE and transferred onto polyvinylidene fluoride membranes. After blocking for 1 h with 5% skim milk, the proteins on the membranes were incubated overnight at 4°C with primary VGF antibody. After three washes with Tris-buffered saline with Tween 20, the proteins on the membranes were incubated for 1 h with the horseradish peroxidase-conjugated secondary antibody and developed using chemiluminescent substrates. Fusion Edge software (Vilber Lourmat) was used for quantification.

2.13 | Transmission Electron Microscopy

MIN6-K8 cells were fixed with a mixture of 2% paraformaldehyde and 2.5% glutaraldehyde overnight at 4°C and were then embedded in epoxy resin. Ultrathin sections mounted on gold meshes were stained with uranyl acetate–lead citrate and examined using an HT7700 transmission electron microscope (Hitachi) [23]. The sizes and diameters of insulin granules (12 sections per group) of each group of MIN6-K8 cells were measured.

2.14 | Islet Isolation

Mouse pancreatic islets were isolated as described previously [24]. Each minced pancreas was digested in 10 mL of collagenase P (1 mg/mL in Hank's balanced salt solution; Roche Diagnostics) for 15 min at 37°C. The pellet was resuspended in RPMI-1640 supplemented with 10% FBS, 1% penicillin–streptomycin, 2 mM glutamine, and 11 mM glucose. Pancreatic islets were selected under a stereomicroscope.

2.15 | Insulin Content in MIN6-K8 Cells and Islets

To measure proinsulin and insulin contents, MIN6-K8 cells and islets were treated with 1% hydrochloric acid-ethanol for 24 h at 4°C after ultrasonic homogenization. Mouse insulin and proinsulin were measured using ultra-sensitive Mouse Insulin (Morinaga Institute of Biological Science) and Proinsulin (ALPCO Diagnostics, Cosmo Bio) enzyme-linked immunosorbent assay kits, respectively. Protein content was determined using Protein Assay Kit I (Bio-Rad Laboratories).

2.16 | Perifusion Assay

The perifusion assay was performed in MIN6-K8 cells and isolated mouse islets as described previously [9, 25]. After pre-incubation in HKRB containing 2.8 mM glucose (30 min for MIN6-K8 cells and 1 h for islets), the MIN6-K8 cells or islets were loaded onto a 0.2-μm

syringe filter (Sartorius). The filter was connected to a peristaltic pump with a flow rate of 1 mL/min and then equilibrated with HKRB containing 2.8 mM glucose for 5 min before the medium was changed to 2.8 mM glucose containing 35 mM KCl or 11.2 mM glucose containing 35 mM KCl and 100 μM diazoxide. The insulin release ratios at different time points were normalized against the insulin content at 0 min.

3 | Statistical Analysis

Statistical analyses were performed on GraphPad Prism 7 statistical software (GraphPad) using one-way analysis of variance (ANOVA) and Tukey's multiple comparisons test as well as unpaired two-tailed Student's *t*-test. Outliers in all experiments were identified using the ROUT method on Prism. All data are expressed as the mean ± s.e.m. Statistical significance was set at $p < 0.05$.

4 | Results

4.1 | VGF$^{\triangle NERP\text{-}4}$ Reduces Insulin Storage

We studied five groups to investigate the roles of NERP-4 in β-cell granulogenesis (Figure 1a; siSCR, si*Vgf*, si*Vgf*+*Vgf*^{full}, si*Vgf*+*Vgf*$^{\triangle Nerp\text{-}4}$, and si*Vgf*+*Vgf*$^{\triangle Nerp\text{-}4}$+NERP-4 administration). Compared with the scrambled control short interfering RNA (siRNA) group (siSCR), si*Vgf* reduced the *Vgf* mRNA level by 64% (Figure S1a). Transfection of pcDNA3.1-full-length *Vgf* (*Vgf*^{full}) into si*Vgf*-treated MIN6-K8 cells restored the VGF protein level to a similar degree as that in siSCR (Figure 1b). Transfection of pcDNA3.1-*Nerp-4*–deleted *Vgf* (*Vgf*$^{\triangle Nerp\text{-}4}$) into si*Vgf* also restored the *Vgf* mRNA level to a similar degree as that in siSCR (Figure S1a) but did not restore the VGF protein level (Figure 1b). SNAT2 mRNA levels were similar in all groups (Figure S1b). We confirmed NERP-4 deletion in si*Vgf* and *Vgf*$^{\triangle Nerp\text{-}4}$ and its expression in *Vgf*^{full} by immunocytochemistry (Figure 1c).

si*Vgf*, *Vgf*^{full}, or *Vgf*$^{\triangle Nerp\text{-}4}$ did not affect the *Ins1* or *Ins2* mRNA level (Figure S1c). Transmission electron microscopy revealed that si*Vgf* reduced the number and size of insulin granules (Figure 1d–f). *Vgf*^{full} restored both, whereas *Vgf*$^{\triangle Nerp\text{-}4}$ did not. Both si*Vgf* and *Vgf*$^{\triangle Nerp\text{-}4}$ reduced insulin content, which was restored by *Vgf*^{full} (Figure 1g). NERP-4 administration to *Vgf*$^{\triangle Nerp\text{-}4}$ did not restore the VGF protein level, number, or size of insulin granules, or insulin content (Figure 1b,d–g). These results suggest that *Vgf*$^{\triangle Nerp\text{-}4}$ exhibits defective insulin granule formation and that NERP-4 administration has no effect on granule formation. Both si*Vgf* and *Vgf*$^{\triangle Nerp\text{-}4}$ reduced insulin secretion, which was restored by *Vgf*^{full} and NERP-4 administration to *Vgf*$^{\triangle Nerp\text{-}4}$ (Figure 1h). The proinsulin/insulin ratio increased in both si*Vgf* and *Vgf*$^{\triangle Nerp\text{-}4}$ compared with siSCR (Figure 1i). VGF$^{\triangle NERP\text{-}4}$ has an impaired function as a granin protein.

4.2 | NERP-4 Region Is Critical for VGF Function in Insulin Granule Trafficking

We presumed that VGF$^{\triangle NERP\text{-}4}$ caused defective granule function. We first studied the cytoplasmic distributions of insulin, VGF, and the *trans*-Golgi marker TGN38 by immunostaining. si*Vgf* reduced the insulin-positive area and caused insulin accumulation in the TGN38-positive area (Figure 2a–c), suggesting impaired granule sedimentation and localization in VGF-deficient cells. *Vgf*^{full} restored the diffuse and punctate insulin staining throughout the cytosol, but neither *Vgf*$^{\triangle Nerp\text{-}4}$ nor NERP-4 administration to *Vgf*$^{\triangle Nerp\text{-}4}$ restored this insulin staining pattern (Figure 2a–c). si*Vgf* reduced the VGF-positive area (Figure 2d,e). *Vgf*^{full} restored the VGF-positive area, but neither *Vgf*$^{\triangle Nerp\text{-}4}$ nor NERP-4 administration to *Vgf*$^{\triangle Nerp\text{-}4}$ did (Figure 2d,e). The total VGF-positive area in siSCR was 2.7-fold bigger than the VGF area with TGN38 colocalization, which indicates that VGF diffused throughout the cytosol (Figure 2f,g). si*Vgf* retained VGF in the TGN38-positive area (Figure 2f,g). *Vgf*^{full} restored VGF distribution throughout the cytosol, whereas *Vgf*$^{\triangle Nerp\text{-}4}$ or NERP-4 administration to *Vgf*$^{\triangle Nerp\text{-}4}$ did not (Figure 2f,g).

Insulin is released from β cells in a biphasic manner that reflects mobilization of distinct pools of insulin granules. To investigate whether VGF$^{\triangle NERP\text{-}4}$ could recruit insulin granules potently and persistently, we studied the biphasic insulin secretion response by a perifusion assay [9, 26] using MIN6-K8 cells transfected with *Vgf*^{full} or *Vgf*$^{\triangle Nerp\text{-}4}$ (Figure 3a). We examined the first-phase insulin secretion by adenosine triphosphate (ATP)-mediated closure of K_{ATP} channels via direct membrane depolarization, which was achieved through 35 mM KCl stimulation in 2.8 mM basal glucose. To examine the second-phase insulin secretion, which is independent of the K_{ATP} channel, we used diazoxide to open the K_{ATP} channel in the presence of stimulatory 35 mM KCl and 11.2 mM glucose. Both *Vgf*^{full} and *Vgf*$^{\triangle Nerp\text{-}4}$ exhibited equally potent first-phase insulin secretion, while *Vgf*$^{\triangle Nerp\text{-}4}$ decreased the second-phase insulin secretion compared with *Vgf*^{full} (Figure 3b,c). Collectively, these findings demonstrate that VGF$^{\triangle NERP\text{-}4}$ exhibits insufficient activity on the VGF-mediated sustained replenishment of insulin granules.

4.3 | NERP-4 Acts on β-Cell Maintenance

We investigated the roles of NERP-4 in β-cell maintenance among the five groups shown in Figure 1a. si*Vgf* reduced β-cell viability (Figure 4a). Both *Vgf*^{full} and NERP-4 administration to *Vgf*$^{\triangle Nerp\text{-}4}$ augmented cell viability, whereas *Vgf*$^{\triangle Nerp\text{-}4}$ alone did not (Figure 4a). Mitochondrial dysfunction in diabetic β cells disrupts insulin release. We have previously reported that administration of NERP-4 to diabetic β cells reversed mitochondrial dysfunction [15]. si*Vgf* reduced intracellular ATP production induced by high glucose stimulation (Figure 4b). Both *Vgf*^{full} and NERP-4 administration to *Vgf*$^{\triangle Nerp\text{-}4}$ augmented ATP production, while *Vgf*$^{\triangle Nerp\text{-}4}$ alone did not (Figure 4b). Chronic excess administration of free fatty acids triggers oxidative and ER stress, leading to β-cell dysfunction [27]. We analyzed the oxidants and ER stress following palmitate treatment in the five groups (Figure 4c). si*Vgf* increased the production of oxidants (Figure 4d) and the mRNA levels of ER stress markers including *Grp78, Chop*, *Xbp-1*, *Atf4*, and *Atf6* (Figure 4e–i). Both *Vgf*^{full} and NERP-4 administration to *Vgf*$^{\triangle Nerp\text{-}4}$ reversed these changes, whereas *Vgf*$^{\triangle Nerp\text{-}4}$ alone did not (Figure 4d–i). Collectively, these findings indicate that

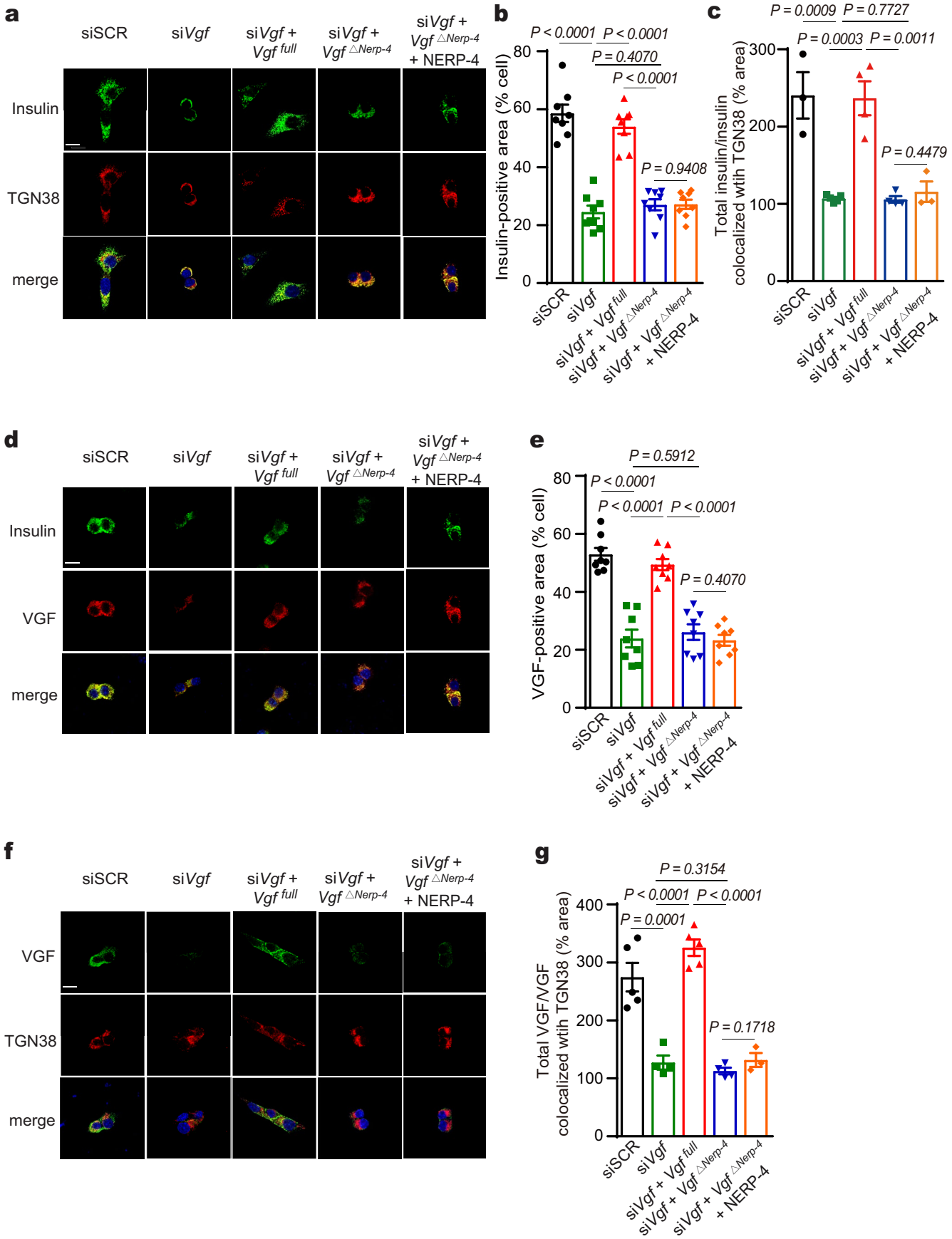

FIGURE 2 | Legend on next page.

FIGURE 2 | NERP-4 is involved in insulin granule trafficking. (a) Representative immunostaining of insulin, TGN38, and DAPI in MIN6-K8 cells ($n = 8$ areas per group). (b) Quantification of insulin-positive area ($n = 8$ areas per group). (c) Area ratio of total insulin/insulin co-localized with TGN38 ($n = 3$ or 5 areas per group). (d) Representative immunostaining of insulin and VGF in MIN6-K8 cells ($n = 8$ areas per group). (e) Quantification of VGF-positive area ($n = 8$). (f) Representative immunostaining of VGF, TGN38, and DAPI ($n = 8$ areas per group). (g) Area ratio of total VGF/VGF co-localized with TGN38 ($n = 4$ or 5 areas per group). Representative results of two independent experiments (a–g). Data are presented as the mean ± s.e.m. (b, c, e, g). One-way ANOVA and Tukey's multiple comparisons test (b, c, e, g). Scale bars, 10 μm (a, d, f).

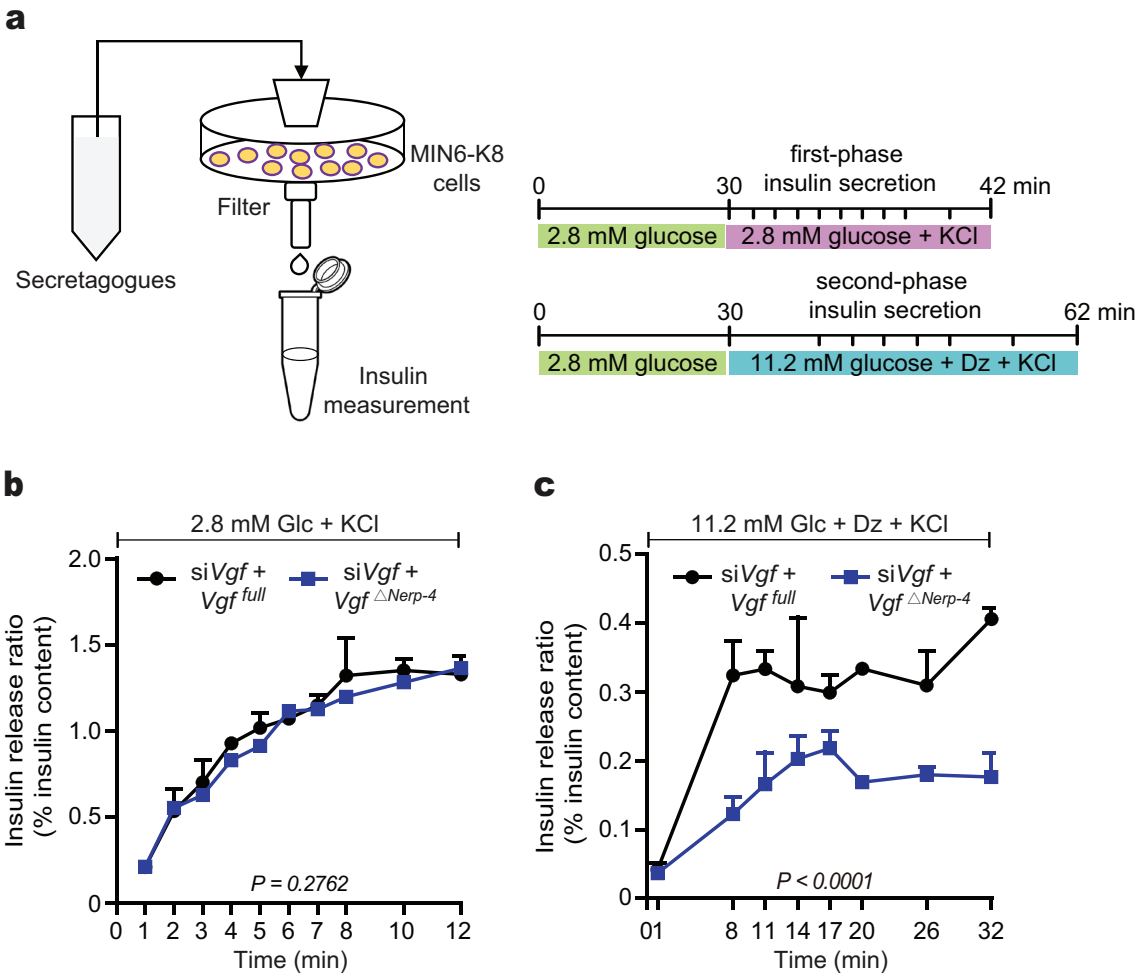

FIGURE 3 | NERP-4 deletion impairs the second-phase insulin secretion and proinsulin processing. (a) Schematic and time course for the perifusion assay of MIN6-K8 cells. (b, c) First-phase insulin secretion from MIN6-K8 cells stimulated with 2.8 mM glucose containing 35 mM KCl (b) and second-phase insulin secretion stimulated with 11.2 mM glucose containing 100 μM diazoxide (Dz) and 35 mM KCl (c) ($n = 3$). Representative results of two independent experiments (b, c). Data are presented as the mean ± s.e.m. (b, c). One-way ANOVA and Tukey's multiple comparisons test (b, c).

NERP-4 plays roles in mitochondrial maintenance and alleviation of oxidative and ER stress even in $Vgf^{\triangle Nerp\text{-}4}$ β cells with impaired granulogenesis.

4.4 | Generation of *Nerp-4*$^{-/-}$ Mice and Characterization of Their Islets

To further study the role of $VGF^{\triangle NERP\text{-}4}$ in β-cell function, we constructed *Nerp-4*$^{-/-}$ mice using CRISPR/Cas9–mediated genome editing (Figures 5a and S2a). Genomic sequencing confirmed the deletion of NERP-4 (Figure S2b). Genetic analyses by PCR showed the deletion of the NERP-4 region in the DNA samples obtained from the tail and hypothalamus of *Nerp-4*$^{-/-}$ mice (Figure S2c). No NERP-4 immunoreactivity was observed in *Nerp-4*$^{-/-}$ mouse islets (Figure 5b). Immunohistochemical analyses showed that the levels of VGF and insulin in *Nerp-4*$^{-/-}$ islets were lower than those in the islets of wild-type (WT) littermates (Figure 5c,d). The plasma insulin levels of *Nerp-4*$^{-/-}$ mice were lower than those of WT littermates (Figure 5e). The *Vgf* mRNA levels in *Nerp-4*$^{-/-}$ and WT islets were similar, whereas the VGF protein levels in *Nerp*-4$^{-/-}$ islets were lower than those in WT islets (Figure 5f,g).

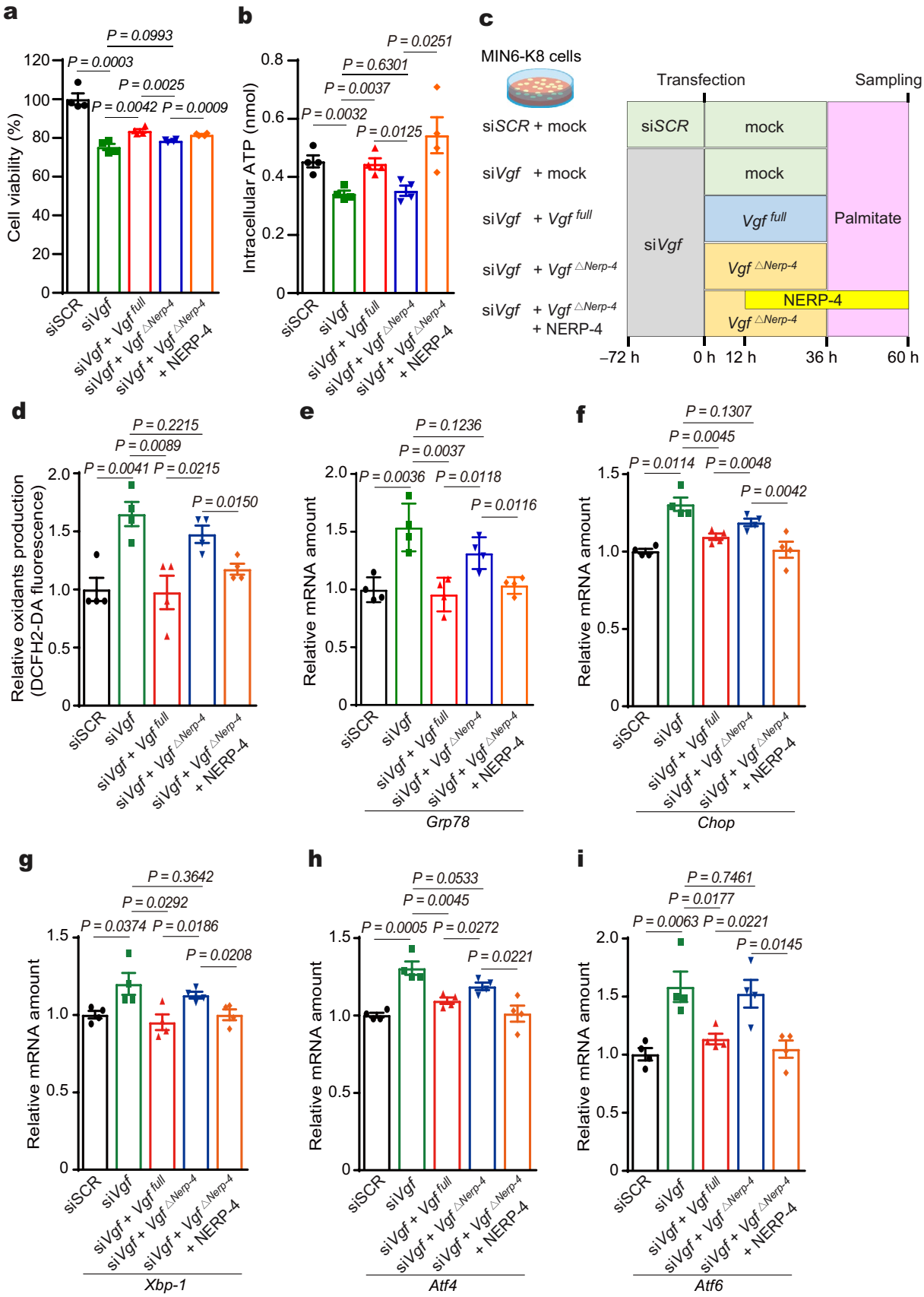

FIGURE 4 | NERP-4 deletion impairs β-cell function and maintenance. (a) Cell viability ($n = 4$). (b) ATP production ($n = 4$). (c) Palmitate was administered for 24 h after Vgf^{full} or $Vgf^{\triangle Nerp\text{-}4}$ transfection. NERP-4 was administered thrice, at 12, 24, and 36 h after $Vgf^{\triangle Nerp\text{-}4}$ transfection. (d) Oxidant production ($n = 4$). (e–i) *Grp78*, *Chop*, *Xbp-1*, *Atf4*, and *Atf6* mRNA levels ($n = 4$). Representative results of two independent experiments (a, b, d–i). Data are presented as the mean ± s.e.m. (a, b, d–i). One-way ANOVA and Tukey's multiple comparisons test (a, b, d–i).

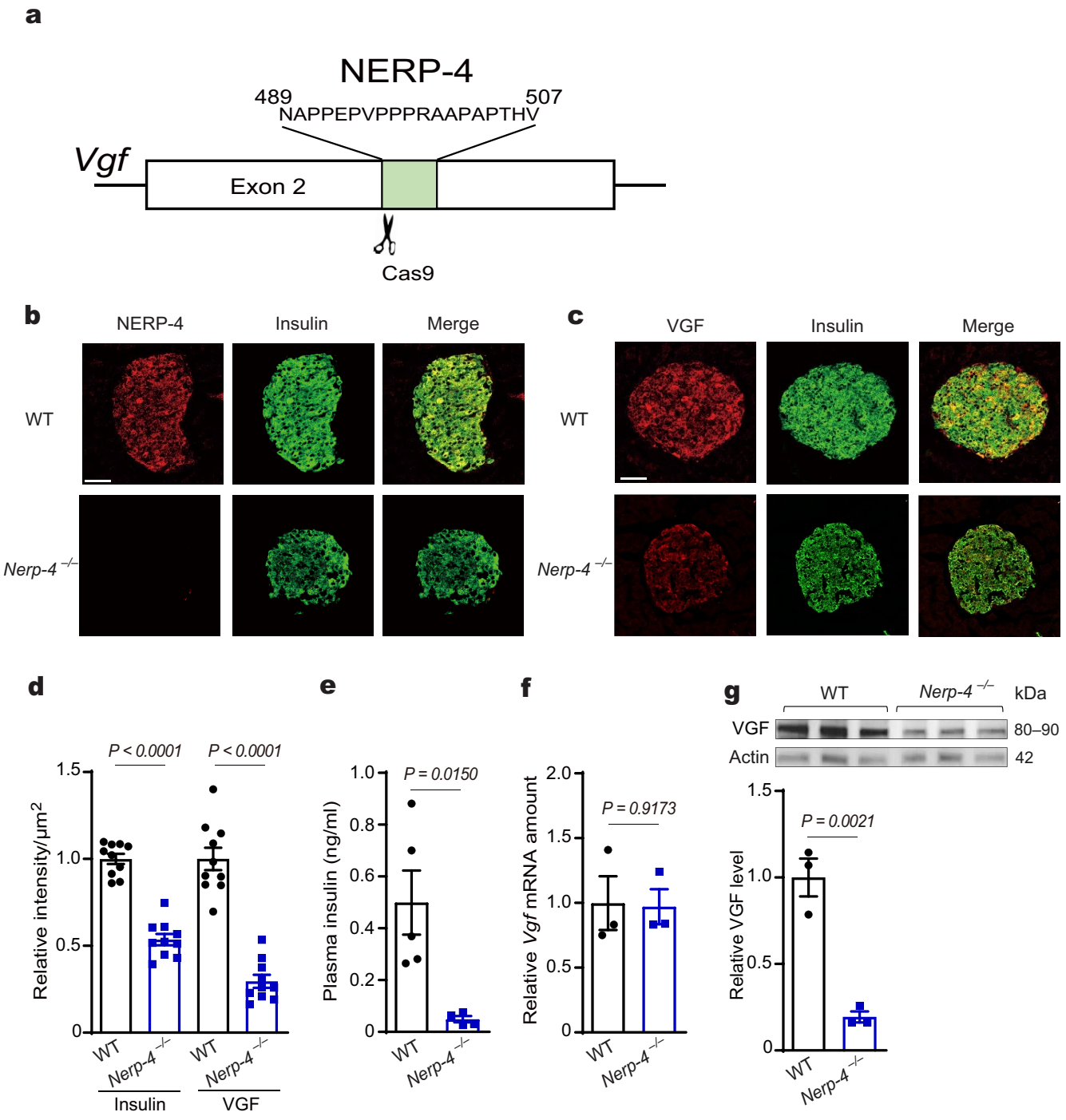

FIGURE 5 | Generation of *Nerp-4*$^{-/-}$ mice and characterization of their islets. (a) Schematic presentation of the CRISPR/Cas9–mediated genome editing strategy to generate *Nerp-4*$^{-/-}$ mice. (b, c) Representative immunostaining of NERP-4 (b) and VGF (c) together with insulin in the islets of WT and *Nerp-4*$^{-/-}$ mice ($n = 3$). (d) Relative fluorescence intensity of insulin and VGF in the islets of WT and *Nerp-4*$^{-/-}$ mice (10 islets from three mice each). (e) Plasma insulin levels in WT and *Nerp-4*$^{-/-}$ mice under *ad libitum* condition ($n = 5, 4$). (f) *Vgf* mRNA levels in the islets of WT and *Nerp-4*$^{-/-}$ mice ($n = 3$). (g) VGF protein levels in the islets of WT and *Nerp-4*$^{-/-}$ mice ($n = 3$). Representative results of two independent experiments (b–g). Data are presented as the mean ± s.e.m. (d–g). Unpaired two-sided *t*-test (d–g). Scale bars, 50 μm (b, c).

4.5 | *Nerp-4*$^{-/-}$ Islets Have Impaired Mobilization of Secretory Granules

The mRNA levels of *Ins1* and *Ins2* did not differ between *Nerp-4*$^{-/-}$ and WT islets (Figure 6a). The insulin content in *Nerp-4*$^{-/-}$ islets was lower than that in WT islets (Figure 6b). The proinsulin/insulin ratio was higher in *Nerp-4*$^{-/-}$ islets (Figure 6c). We conducted the islet perifusion assay according to the procedure described in Figure 3a, except for the 1 h pre-incubation step in 2.8 mM glucose. The first-phase insulin secretion was similar between *Nerp-4*$^{-/-}$ and WT islets, whereas the second-phase insulin secretion decreased

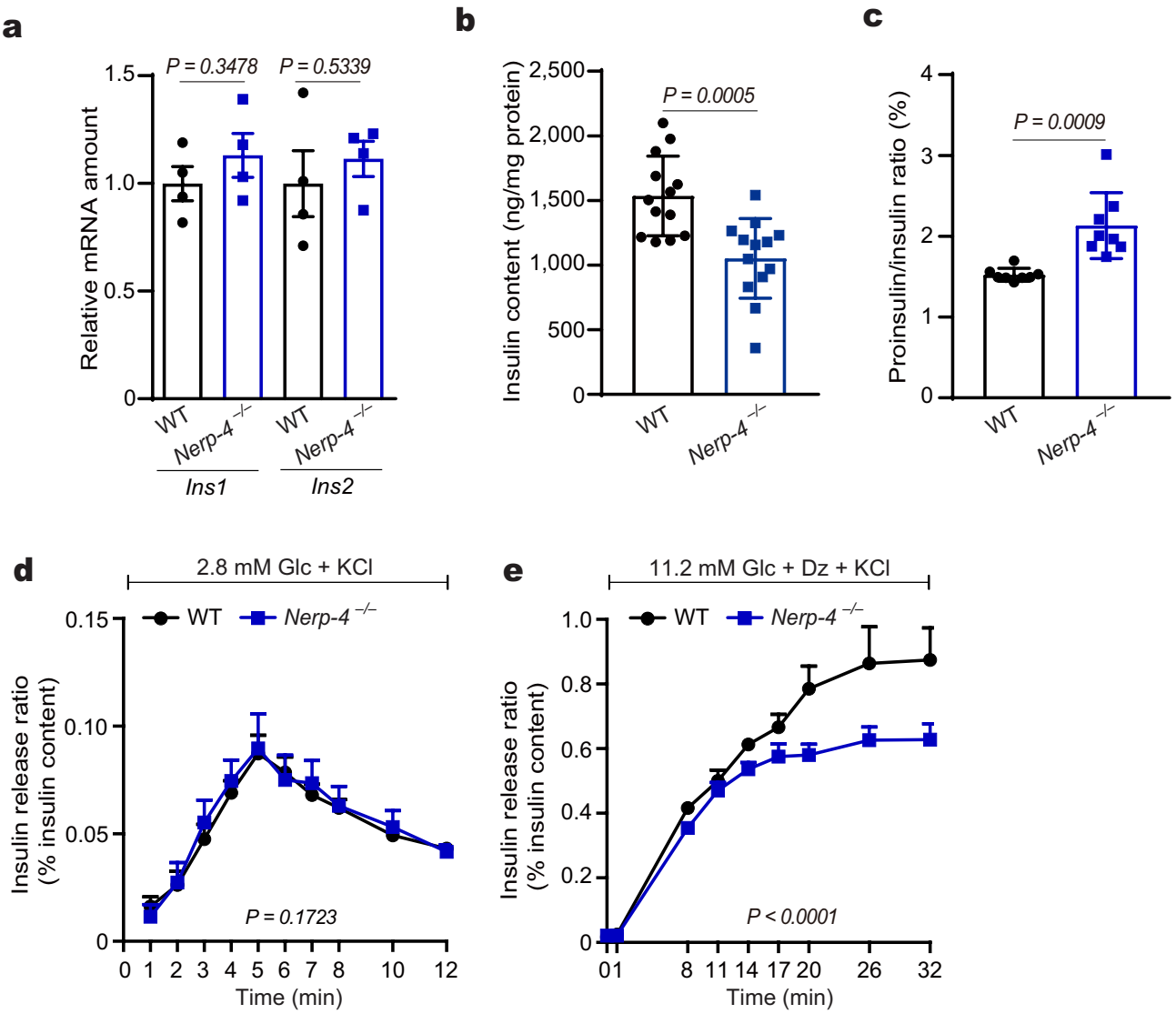

FIGURE 6 | *Nerp-4*$^{-/-}$ mouse islets have impaired second-phase insulin secretion. (a) *Ins1* and *Ins2* mRNA levels in the islets of WT and *Nerp-4*$^{-/-}$ mice ($n = 3$). (b) Insulin contents in the islets of WT and *Nerp-4*$^{-/-}$ mice ($n = 13$). (c) Proinsulin/insulin ratio in WT and *Nerp-4*$^{-/-}$ islets ($n = 8$). (d, e) First-phase insulin secretion from WT and *Nerp-4*$^{-/-}$ islets stimulated with 2.8 mM glucose containing 35 mM KCl (d) and second-phase insulin secretion from islets stimulated with 11.2 mM glucose containing 100 μM Dz and 35 mM KCl (e) ($n = 3$). Representative results of two independent experiments (a, d, e). Representative results of two independent experiments (b, c). Data are presented as the mean ± s.e.m. (a–e). Unpaired two-sided *t*-test (a–c). One-way ANOVA and Tukey's multiple comparisons test (d–e).

in *Nerp-4*$^{-/-}$ islets compared with WT islets (Figure 6d,e). Collectively, the results show that *Nerp-4*$^{-/-}$ islets had lower insulin content, higher proinsulin ratio, and impaired second-phase insulin secretion, consistent with the findings observed in *Vgf*$^{\Delta Nerp\text{-}4}$ β cells.

4.6 | NERP-4 Is Reduced in Diabetes Mellitus

To investigate whether NERP-4 is related to diabetes pathogenesis, we studied NERP-4 immunoreactivity in the islets of 20 patients with type 2 diabetes mellitus (T2DM). Both NERP-4 and insulin immunoreactivities were reduced in the patients (Figure 7a,b). The fluorescent intensity of NERP-4 relative to insulin was reduced (Figure 7c).

5 | Discussion

We have previously demonstrated that NERP-4 neutralization in isolated mouse islets reduced insulin secretion and β-cell viability [15]. In the current study, VGF$^{\Delta NERP\text{-}4}$ exhibited similar results (Figure 8). Notably, VGF$^{\Delta NERP\text{-}4}$ impaired β-cell granulogenesis and insulin maturation, storage, and transport. These findings are comparable to those obtained in the si*Vgf* experiments in the current study.

Granins produced in endocrine and neuronal tissues function as granule-forming proteins and peptide precursors. They self-aggregate at the *trans*-Golgi network, leading to productive sorting and concentrating the granule contents in β cells [28, 29]. Proinsulin, along with VGF and chromogranin A and

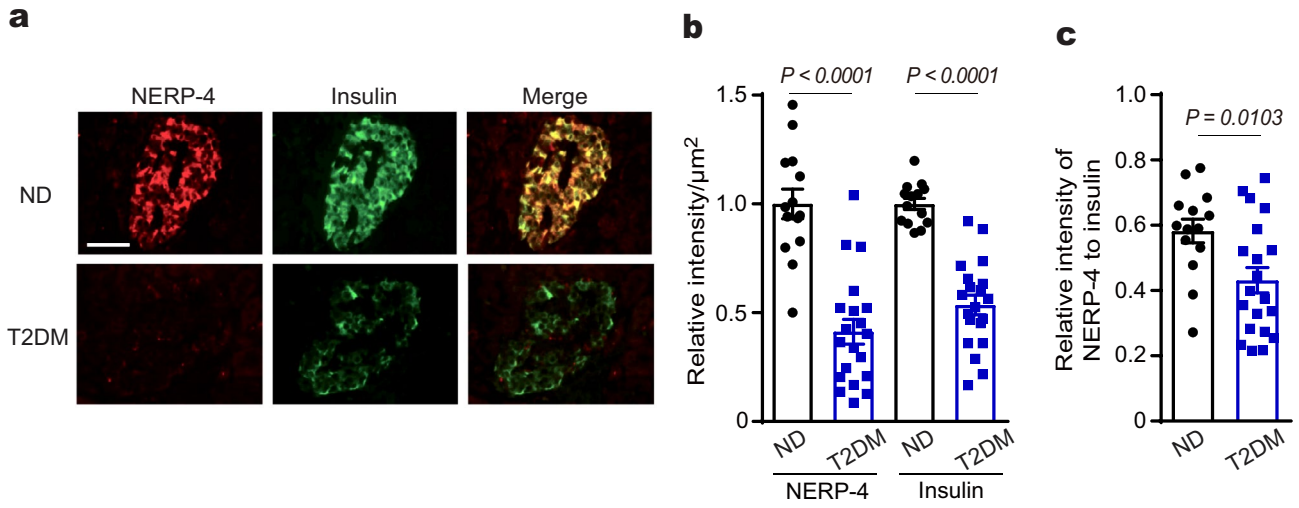

FIGURE 7 | NERP-4 is reduced in patients with type 2 diabetes mellitus. (a) Representative immunostaining of NERP-4 and insulin in the islets of non-diabetes individuals (ND) ($n = 14$) and patients with type 2 diabetes mellitus (T2DM) ($n = 20$). (b) Fluorescent intensity of NERP-4 and insulin in the islets of the ND and T2DM. (c) Relative fluorescent intensity of NERP-4 to insulin in the islets. Data are presented as the mean ± s.e.m. (b, c). Unpaired two-tailed Student's t-test (b, c). Scale bars, 50 μm (a).

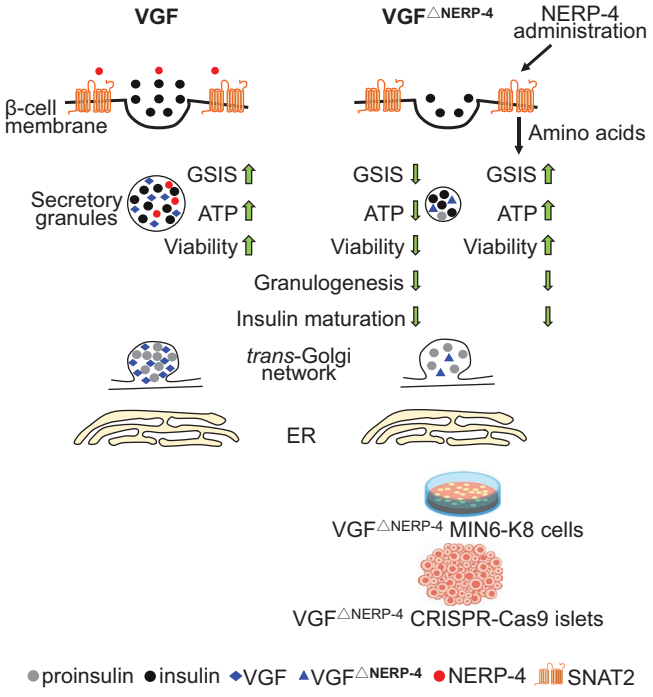

FIGURE 8 | Schematic representation of the mechanism underlying VGF$^{\triangle NERP\text{-}4}$–induced β-cell impairment. VGF functions as a granin protein in β-cell granulogenesis and as a precursor of NERP-4. VGF$^{\triangle NERP\text{-}4}$ impairs granulogenesis and replenishment of insulin granule stores in the second-phase insulin secretion. VGF$^{\triangle NERP\text{-}4}$ also reduces insulin content and β-cell viability. SNAT2 expression is preserved in VGF$^{\triangle NERP\text{-}4}$ β cells. NERP-4 administration to VGF$^{\triangle NERP\text{-}4}$ β cells acts on SNAT2, thereby enhancing GSIS, ATP production, and cell viability but not granulogenesis or insulin maturation.

B, is sequestered to the immature secretory granules that bud off from the *trans*-Golgi network. VGF depletion in rat insulinoma-derived INS1-832/3 cells reduced the number and size of secretory granules [9]. β-cell–specific VGF depletion in mouse islets also caused a defect in granule replenishment, hampering the secretion of newly synthesized granules during the second phase of glucose-stimulated insulin secretion (GSIS) [9]. In the current study, full-length *Vgf* transfection restored VGF mRNA and protein levels to those in the scramble control siRNA group. This validated the sufficient expression efficacy in transfection experiments. VGF$^{\triangle NERP\text{-}4}$ in both MIN6-K8 cells and CRISPR-Cas9–designed mouse islets expressed insulin and VGF mRNA levels similar to those in the respective controls but exhibited reduced protein levels. NERP-4 administration to VGF$^{\triangle NERP\text{-}4}$ did not restore these reductions. Collectively, these results show that deletion of the NERP-4 region in VGF causes reduced insulin and VGF levels.

The NERP-4 region (VGF 489–507 in mice) consists of 19 amino acids, of which eight are proline residues. The pyrrolidine ring in proline generates steric hindrance in protein backbones. This unique structural characteristic confers the proline-rich region with the ability to engage in protein–protein interactions [30]. The AlphaFold Protein Structure Database [31] predicts that VGF is a natively unfolded protein that is very flexible and has no stable conformation (Figure S2). The NERP-4 region forms a bending loop in the VGF structure. NERP-4 deletion from VGF could cause its structural instability and lower the binding ability to other granin-forming substances, possibly leading to reduced VGF amounts and impaired granulogenesis. A proteomic analysis of MIN6 cells has identified 211 proteins in their insulin granules [19]. These proteins are thought to have interdependent relationships to regulate granule biogenesis, trafficking, and GSIS [10]. For example, chromogranin B deficiencies in β cells reduced the VGF protein level and impaired proinsulin processing and GSIS in vitro and in vivo [4, 32]. Further investigations may delineate that VGF$^{\triangle NERP\text{-}4}$ affects storage of other granule proteins.

We demonstrated that NERP-4 administration to MIN6-K8 cells and isolated mouse islets treated with palmitate enhanced GSIS

and maintained β-cell viability via the NERP-4–SNAT2 axis [15]. Conversely, NERP-4 neutralization suppressed the antioxidative response and increased ER stress. In the current study, NERP-4 administration to VGF$^{\triangle NERP\text{-}4}$ MIN6-K8 cells did not reverse the impaired granulogenesis or reduced insulin and VGF amounts but restored the changes in GSIS, β-cell viability, and oxidative and ER stress. These indicate that exogeneous NERP-4 can act on insulin secretion and β-cell maintenance under conditions wherein granulogenesis is impaired while SNAT2 expression is preserved in VGF$^{\triangle NERP\text{-}4}$.

Proinsulin is ultimately converted to insulin and C-peptide in the secretory granules via proteolytic cleavages by PC1/3 and PC2 [2, 19, 33, 34]. Granin-mediated aggregation in the secretory granules builds an appropriate milieu for optimal proteolytic cleavage. The increase in the proinsulin/insulin ratio induced by VGF$^{\triangle NERP\text{-}4}$ implies insufficient insulin maturation.

Insulin secretion is biphasic. During the second-phase insulin secretion, the sustained replenishment of the insulin granule pool maintains the full insulin secretory capacity of β cells. In the perifusion assay of the present study, both VGF$^{\triangle NERP\text{-}4}$ MIN6-K8 cells and islets exhibited reduced second-phase insulin secretion. TGN38 immunostaining in VGF$^{\triangle NERP\text{-}4}$ MIN6-K8 cells revealed restricted insulin distribution around the *trans*-Golgi network. These findings suggest that VGF$^{\triangle NERP\text{-}4}$ results in impaired granule sedimentation and trafficking.

To explore whether NERP-4 reduction is linked to diabetes mellitus, we searched for human VGF mutation in the ClinVar database, which aggregates information about genetic variation and its relationship to human health. No VGF mutation related to diabetes mellitus has been registered. The present immunohistochemical analyses on the islets of patients with T2DM revealed a reduction of the NERP-4 to insulin ratio, suggesting that NERP-4 reduction may be involved in diabetes pathogenesis.

Our current study has some limitations. First, we studied mice carrying NERP-4 deletion in the systemic tissues. Previous studies of systemic *Vgf*$^{-/-}$ mice exhibited reductions in plasma insulin, pituitary gonadotropin contents, body weight, and peripheral fat storage, and elevation in energy expenditure [35, 36]. They were small, hyperactive, and infertile. VGF protein amount in *Nerp-4*$^{-/-}$ mouse islets was reduced to 19.4% of that of WT mouse islets. We have found that *Nerp-4*$^{-/-}$ mice are also small, hyperactive, and infertile. These findings suggest that the phenotype of systemic *Nerp-4*$^{-/-}$ mice is close to *Vgf*$^{-/-}$ mice. We need to investigate systemic and metabolic features of *Nerp-4*$^{-/-}$ mice with much future research. Second, VGF interacts with other granins for the efficient delivery and trafficking of proinsulin and requisite maturation factors such as prohormone convertases into the budding granule [4, 9]. In the current study, we demonstrated the structural importance of the NERP-4 region in VGF in granulogenesis. Future protein–protein interaction experiments using VGF$^{\triangle NERP\text{-}4}$ and chromogranins could further elucidate the pathogenic implication of VGF$^{\triangle NERP\text{-}4}$ in β-cell biology.

Overall, VGF$^{\triangle NERP\text{-}4}$ exhibited two defective roles of VGF as a granin protein and an NERP-4 precursor. The current study extends our understanding of the roles of VGF in the context of granulogenesis and function as a peptide precursor in β cells.

Author Contributions

Weidong Zhang: investigation; data curation; visualization; methodology; funding acquisition; writing – original draft; writing – review and editing. **Yuki Nakazato:** investigation; data curation; methodology; writing – review and editing. **Naoto Minamino:** supervision; methodology; writing – review and editing. **Nobuaki Okumura:** supervision; methodology; writing – review and editing. **Ayako Miura:** data curation; visualization; methodology; writing – original draft. **Takefusa Tarusawa:** investigation; data curation. **Hiroki Mizukami:** data curation; methodology; writing – review and editing. **Hideyuki Sakoda:** visualization; methodology; writing – review and editing. **Masamitsu Nakazato:** supervision; funding acquisition; writing – original draft; writing – review and editing.

Acknowledgments

The authors thank Junichi Miyazaki (The University of Osaka) for providing MIN6-K8 cells. This study was supported in part by the Japan Society for the Promotion of Science (JSPS) KAKENHI (25293216, 15K09439) (to M. N.), and 22K06004 (to W. Z.), the Agency for Medical Research and Development–Core Research for Evolutional Science and Technology (AMED-CREST, 19gm0610016h0006) (to M. N.), the Mochida Memorial Foundation for Medical and Pharmaceutical Research (to W. Z.), the Takeda Science Foundation for Medical Research (to W. Z.), Novo Nordisk Pharma Research Grant (Japan Society for the Study of Obesity) (to W. Z.), Japan Diabetes Society Research Grant (to W. Z.), Manpei Suzuki Diabetes Foundation for Diabetes Research (to W. Z.), and a Clinical Research Support Grant from University of Miyazaki Hospital (to Y. N.).

Funding

This work was supported by MEXT | Japan Society for the Promotion of Science (JSPS) (25293216, 15K09439, 22K06004) the Agency for Medical Research and Development-Core Research for Evolutional Science and Technology (19gm0610016h0006) the Mochida Memorial Foundation for Medical and Pharmaceutical Research the Takeda Science Foundation for Medical Research. Novo Nordisk Pharma Research Grant Japan Diabetes Society Research Grant Manpei Suzuki Diabetes Foundation for Diabetes Research Clinical Research Support Grant from the University of Miyazaki Hospital.

Conflicts of Interest

The authors declare no conflicts of interest.

Data Availability Statement

The data needed to reproduce the findings described in this manuscript can be found in the manuscript figures and Supporting Information, and is available from the authors upon reasonable request.

References

1. L. Orci, P. Halban, M. Amherdt, M. Ravazzola, J. D. Vassalli, and A. Perrelet, "Nonconverted, Amino Acid Analog-Modified Proinsulin Stays in a Golgi-Derived Clathrin-Coated Membrane Compartment," *Journal of Cell Biology* 99 (1984): 2187–2192.

2. C. J. Rhodes and P. A. Halban, "Newly Synthesized Proinsulin/Insulin and Stored Insulin Are Released From Pancreatic β Cells Predominantly via a Regulated, Rather Than a Constitutive, Pathway," *Journal of Cell Biology* 105 (1987): 145–153.

3. A. Bartolomucci, R. Possenti, S. K. Mahata, R. Fischer-Colbrie, Y. P. Loh, and S. R. J. Salton, "The Extended Granin Family: Structure, Function, and Biomedical Implications," *Endocrine Reviews* 32 (2011): 755–797.

4. S. C. Bearrows, C. J. Bauchle, M. Becker, J. M. Haldeman, S. Swaminathan, and S. B. Stephens, "Chromogranin B Regulates Early-Stage Insulin Granule Trafficking From the Golgi in Pancreatic Islet β-Cells," *Journal of Cell Science* 132 (2019): jcs231373.

5. M. Omar-Hmeadi and O. Idevall-Hagren, "Insulin Granule Biogenesis and Exocytosis," *Cellular and Molecular Life Sciences* 78 (2021): 1957–1970.

6. N. Canu, R. Possenti, A. S. Ricco, M. Rocchi, and A. Levi, "Cloning, Structural Organization Analysis, and Chromosomal Assignment of the Human Gene for the Neurosecretory Protein VGF," *Genomics* 45 (1997): 443–446.

7. K. B. Helle, "The Granin Family of Uniquely Acidic Proteins of the Diffuse Neuroendocrine System: Comparative and Functional Aspects," *Biological Reviews* 79 (2004): 769–794.

8. J. E. Lewis, J. M. Brameld, and P. H. Jethwa, "Neuroendocrine Role for VGF," *Frontiers in Endocrinology* 6 (2015): 3.

9. S. B. Stephens, R. J. Edwards, M. Sadahiro, et al., "The Prohormone VGF Regulates β Cell Function via Insulin Secretory Granule Biogenesis," *Cell Reports* 20 (2017): 2480–2489.

10. N. Norris, B. Yau, and M. A. Kebede, "Isolation and Proteomics of the Insulin Secretory Granule," *Metabolites* 11 (2021): 288.

11. S. Hannedouche, V. Beck, J. Leighton-Davies, et al., "Identification of the C3a Receptor (C3AR1) as the Target of the VGF-Derived Peptide TLQP-21 in Rodent Cells," *Journal of Biological Chemistry* 288 (2013): 27434–27443.

12. A. S. Moin, H. Yamaguchi, M. Rhee, et al., "Neuroendocrine Regulatory Peptide-2 Stimulates Glucose-Induced Insulin Secretion *in Vivo* and *in Vitro*," *Biochemical and Biophysical Research Communications* 428 (2012): 512–517.

13. P. Petrocchi-Passeri, C. Cero, A. Cutarelli, et al., "The VGF-Derived Peptide TLQP-62 Modulates Insulin Secretion and Glucose Homeostasis," *Journal of Molecular Endocrinology* 54 (2015): 227–239.

14. S. B. Stephens, J. C. Schisler, H. E. Hohmeier, et al., "A VGF-Derived Peptide Attenuates Development of Type 2 Diabetes via Enhancement of Islet Beta-Cell Survival and Function," *Cell Metabolism* 16 (2012): 33–43.

15. W. Zhang, A. Miura, A. S. Moin, et al., "The NERP-4–SNAT2 Axis Regulates Pancreatic β-Cell Maintenance and Function," *Nature Communications* 14 (2023): 8158.

16. M. Iwasaki, K. Minami, T. Shibasaki, T. Miki, J. I. Miyazaki, and S. Seino, "Establishment of New Clonal Pancreatic β-Cell Lines (MIN6-K) Useful for Study of Incretin/Cyclic Adenosine Monophosphate Signaling," *Journal of Diabetes Investigation* 1 (2010): 137–142.

17. G. Han, H. Takahashi, N. Murao, et al., "Glutamate Is an Essential Mediator in Glutamine-Amplified Insulin Secretion," *Journal of Diabetes Investigation* 12 (2021): 920–930.

18. M. Hashim, N. Yokoi, H. Takahashi, et al., "Inhibition of SNAT5 Induces Incretin-Responsive State From Incretin-Unresponsive State in Pancreatic β-Cells: Study of β-Cell Spheroid Clusters as a Model," *Diabetes* 67 (2018): 1795–1806.

19. N. Norris, B. Yau, C. Famularo, et al., "Optimized Proteomic Analysis of Insulin Granules From MIN6 Cells Identifies Scamp3, a Novel Regulator of Insulin Secretion and Content," *Diabetes* 73 (2024): 2045–2054.

20. H. Sies, V. V. Belousov, N. S. Chandel, et al., "Defining Roles of Specific Reactive Oxygen Species (ROS) in Cell Biology and Physiology," *Nature Reviews. Molecular Cell Biology* 23 (2022): 499–515.

21. E. Mishiro-Sato, K. Sasaki, T. Matsuo, et al., "Distribution of Neuroendocrine Regulatory Peptide-1 and -2, and Proteolytic Processing of Their Precursor VGF Protein in the Rat," *Journal of Neurochemistry* 114 (2010): 1097–1106.

22. W. Zhang, H. Sakoda, and M. Nakazato, "Neuromedin U Suppresses Insulin Secretion by Triggering Mitochondrial Dysfunction and Endoplasmic Reticulum Stress in Pancreatic β-Cells," *FASEB Journal* 34 (2020): 133–147.

23. S. Z. Hasnain, J. B. Prins, and M. A. McGuckin, "Oxidative and Endoplasmic Reticulum Stress in β-Cell Dysfunction in Diabetes," *Journal of Molecular Endocrinology* 56 (2016): R33–R54.

24. W. Zhang, H. Sakoda, Y. Nakazato, et al., "Neuromedin U Uses Gαi2 and Gαo to Suppress Glucose-Stimulated Ca^{2+} Signaling and Insulin Secretion in Pancreatic β Cells," *PLoS One* 16 (2021): e0250232.

25. W. Zhang, H. Sakoda, K. Shimizu, et al., "Neuromedin U Suppresses Glucose-Stimulated Insulin Secretion in Pancreatic β Cells," *Biochemical and Biophysical Research Communications* 493 (2017): 677–683.

26. P. Gilon, M. A. Ravier, J. C. Jonas, and J. C. Henquin, "Control Mechanisms of the Oscillations of Insulin Secretion *in Vitro* and *in Vivo*," *Diabetes* 1 (2002): S144–S151.

27. W. Cui, J. Ma, X. Wang, W. Yang, J. Zhang, and Q. Ji, "Free Fatty Acid Induces Endoplasmic Reticulum Stress and Apoptosis of β-Cells by Ca^{2+}/Calpain-2 Pathways," *PLoS One* 8 (2013): e59921.

28. W. B. Huttner, H. H. Gerdes, and P. Rosa, "The Granin (Chromogranin/Secretogranin) Family," *Trends in Biochemical Sciences* 16 (1991): 27–30.

29. L. Taupenot, K. L. Harper, and D. T. O'Connor, "The Chromogranin-Secretogranin Family," *New England Journal of Medicine* 348 (2003): 1134–1149.

30. M. P. Williamson, "The Structure and Function of Proline-Rich Regions in Proteins," *Biochemical Journal* 297 (1994): 249–260.

31. J. Jumper, R. Evans, A. Pritzel, et al., "Highly Accurate Protein Structure Prediction With AlphaFold," *Nature* 596 (2021): 583–589.

32. S. Obermüller, F. Calegari, A. King, et al., "Defective Secretion of Islet Hormones in Chromogranin-B Deficient Mice," *PLoS One* 5 (2010): e8936.

33. H. W. Davidson, C. J. Rhodes, and J. C. Hutton, "Intraorganellar Calcium and pH Control Proinsulin Cleavage in the Pancreatic Beta Cell via Two Distinct Site-Specific Endopeptidases," *Nature* 333 (1988): 93–96.

34. S. P. Smeekens, A. G. Montag, G. Thomas, et al., "Proinsulin Processing by the Subtilisin-Related Proprotein Convertases Furin, PC2, and PC3," *Proceedings of the National Academy of Sciences of the USA* 89 (1992): 8822–8826.

35. S. Hahm, T. M. Mizuno, T. J. Wu, et al., "Targeted Deletion of the Vgf Gene Indicates That the Encoded Secretory Peptide Precursor Plays a Novel Role in the Regulation of Energy Balance," *Neuron* 23 (1999): 537–548.

36. E. Watson, S. Fargali, H. Okamoto, et al., "Analysis of Knockout Mice Suggests a Role for VGF in the Control of Fat Storage and Energy Expenditure," *BMC Physiology* 9 (2009): 19.

Supporting Information

Additional supporting information can be found online in the Supporting Information section. **FIGURES S1–S2:** fsb271365-sup-0001-FiguresS1.pdf. **Table S1:** PCR primers and antibodies used in this study.